Journal of The Electrochemical Society, **161** (6) D327-D332 (2014)
0013-4651/2014/161(6)/D327/6/$31.00 © The Electrochemical Society

Physicochemical Characterization of Electrosynthesized PbO_2 Coatings: The Effect of Pb^{2+} Concentration and Current Density

Hailian Bi, Changzhou Yu,* Wei Gao, and Peng Cao[z]

Department of Chemical and Materials Engineering, The University of Auckland, Auckland 1142, New Zealand

This work investigated the effect of Pb^{2+} concentration and current density on the microstructure of PbO_2 coatings. The electrodeposition of PbO_2 was conducted in a traditional acidic nitrate solution containing $Pb(NO_3)_2$ and NaF. Ti coupons pre-coated with a Sb-doped SnO_2 interlayer were used as substrate. At a current density < 40 mA/cm^2, a preferential crystallographic orientation of β (301) was observed in the coatings, which exhibited a pebble-shaped morphology. In this current density range, the concentration did not show significant influence on both morphology and phase composition. At a relatively high current density, the PbO_2 displayed a dominant β (211) texture and a generally rough surface morphology with a small crystallite size. The morphology is sensitive to the corresponding current density and Pb^{2+} concentration. At a very high current density of 100 mA/cm^2, the morphology of PbO_2 was affected substantially by the Pb^{2+}concentration. Flower-like microstructure was observed at 0.1 M Pb^{2+} concentration. It is suggested that a low current density (or low potential polarization) or a sufficiently high Pb^{2+} concentration are necessary for forming compact and dense PbO_2 deposits. In addition, the average crystallite size decreases with increasing deposition current density within a certain range.

Manuscript submitted March 13, 2014; revised manuscript received April 9, 2014. Published April 22, 2014.

Electrode coatings are now widely employed to improve the performance of modern electrochemical technology.[1,2] Lead dioxide (PbO_2), as one of the most typical coatings, has been extensively investigated. It has been applied as an effective catalytic anodic material in many areas such as ozone generation,[3,4] electrowinning of copper,[5,6] manufacture of chemicals[7,8] and waste treatment processes.[9–11] Recently the preparation by electrodeposition of stable PbO_2 coatings on inert substrates (typically titanium or carbon) as an anode material has attracted considerable interest.[2] This is because of its well-proven advantages such as low cost compared to the anodes based on precious metals, good electrical conductivity that is comparable to metals, ease of preparation, high oxygen evolution potential and good stability in corrosive media.[2,12]

PbO_2 coatings are commonly manufactured via an electrochemical deposition process from a solution containing soluble lead (II) ions (i.e. Pb^{2+}). The morphology and phase composition of electrosythesized PbO_2 depend on various parameters such as the electrolytes (concentrations of Pb^{2+}, pH, and anions), substrates (Pt, Au, graphite, carbon, or Ti) and their pretreatment conditions, as well as electrodeposition parameters (current density, potential, temperature and electrode configuration). PbO_2 coatings can be prepared with different phase structures (orthorhombic α-PbO_2, tetragonal β-PbO_2, or a mixture of α and β) and a wide range of surface morphologies (flat, angular, rounded, cauliflower-like, porous and others). Consequently significantly different catalytic activities result.

So far, there are extensive literatures on the electrodeposition of PbO_2; however, the effect of electro-deposition conditions on the morphology and phase structure of the resulting PbO_2 is not well understood – the elucidation is somewhat contradictory. This is because of the wide variety of conditions and control parameters employed in each experiment and the subtle dependence of the form and properties of the coatings on the deposition conditions, which makes it difficult to compare the results from different laboratories. For example, Shen et al.[13] investigated the electrodeposition of PbO_2 films on Pt, Au and Ti substrates from an acidic plating solution containing 0.1 M Pb^{2+} ions. The morphology of the resulting β-PbO_2 coatings largely depends on the current density, which ranged from 2 to 20 mA/cm^2.[13] However, this current-dependence was not supported by Li et al.'s work.[14] Yu et al.[15] studied the electrodeposition of PbO_2 thin film on Ti substrates and identified that the PbO_2 deposits were a mixture of α- and β- phases at higher current densities. By contrast, Ghasemi et al.[16] found that the electrosythesized coatings deposited under constant current density were only composed of β-PbO_2. Considering the ever increasing demand in anodic electrodes that are being widely used in electrochemical conversion of organic contaminations in effluents and other environmental treatments,[17–20] a high-performance PbO_2 electrode deserves further optimisation.

Our previous work[21] explored the electrodeposition of PbO_2 on the Ti substrate with a Sb-doped SnO_2 interlayer (i.e. Ti/SnO_2-Sb) and investigated how deposition time and temperature affect the morphology and microstructure of the obtained PbO_2 films. In this work, we reported a detailed study of the physicochemical characteristics of galvanostatic deposited PbO_2 coatings obtained by varying Pb^{2+} concentration and current density. SnO_2, as an undercoat, has been recently applied on Ti substrate to prepare PbO_2 anodes to improve the stability and electrocatalytic activity.[9,15,22] As confirmed in our previous study, the pre-formed interlayer of SnO_2-Sb on Ti can significantly promoted the subsequent electrochemical deposition of PbO_2 coatings. Thus, a Ti/SnO_2-Sb substrate was also employed as the deposition substrate in this work. The correlation between Pb^{2+} concentration, current density and phase structure, morphological features of PbO_2 coatings were systematically investigated. This study may contribute to a fundamental understanding of the electrodeposition, and also provide a perspective on further possible improvement of the physicochemical properties of PbO_2 coatings.

Experimental

Ti substrate and chemicals.— High-purity Ti coupons (99.5%) with dimensions of 30 mm × 10 mm × 1 mm were selected as the substrates. All chemicals are of reagent grade. Lead nitrate ($Pb(NO_3)_2$, Sigma-Aldrich, ≥ 99%), nitric acid (HNO_3, 70%, Sigma-Aldrich), sodium fluoride (NaF, ≥ 99%, Sigma-Aldrich,), tin chloride ($SnCl_4$, 99%, Aldrich), antimony oxide (Sb_2O_3, ≥ 99.9%, Aldrich), hydrochloric acid (HCl, ≥ 37%, Fluka) and isopropanol (C_3H_8O, ≥ 99.5%, Sigma) were all used as received. All aqueous solutions were freshly prepared with ultra-pure water (electrical resistivity > 18 MΩ cm), obtained from an ELGA water purification system.

Preparation of Ti/SnO_2-Sb substrate.— Ti coupons were polished with 1200-grit SiC paper and ultrasonically cleaned with deionized water and acetone sequentially to remove sand particles and grease. The polished coupons were then etched in 10 wt% boiling oxalic acid for 60 min to thoroughly dissolve TiO_2. This chemical etching was followed immediately by ultrasonic cleaning in ethanol for 30 min. The coupons were simply designated as pre-treated Ti substrates. The SnO_2-Sb interlayers were then prepared by thermal decomposition. The pre-treated Ti substrates were first dipped in a precursor solution containing 3.51 g $SnCl_4$, 0.1048 g Sb_2O_3, 4 mL concentrated HCl

*Electrochemical Society Active Member.
[z]E-mail: p.cao@auckland.ac.nz

and 14 mL isopropanol and dried at 100°C for 10 min followed by 500°C for 10 min. This dipping-and-drying procedure was repeated for six times. Finally the coupons were annealed in a muffle furnace at 500°C for 60 min and were thereafter designated as the Ti/SnO_2-Sb substrates.

Preparation of lead dioxide (PbO_2) coatings.— Ti coupon with an interlayer of SnO_2-Sb prepared by thermal decomposition (i.e. Ti/SnO_2-Sb, as described above in Section 2.1) was used for subsequent electrodeposition. As reported in our previous work,[21] high temperature has an significant effect on the crystallization of PbO_2 deposits and results in a larger crystallite size, pyramid-shaped morphology/structure of PbO_2 coatings. To reduce the influence of temperature on the phase composition of the PbO_2 deposits, we chose 20°C for the electrodeposition of PbO_2, based on our previous report.[21] All of the electrodeposition of PbO_2 was carried out by a galvanostatic method in a 200 mL two-electrode beaker cell at 20°C. The as-prepared Ti/SnO_2-Sb substrate with a working area of 10 mm × 10 mm (marked with an insulating tape) and mounted in a Teflon holder was used as the anode, while a copper plate with an area of 10 mm × 20 mm was employed as the cathode. The inter-electrode gap was 15 mm. The cell was stirred with a PTFE coated magnetic stirrer bar (size: 8 mm × 20 mm) at the stirring rate of 500 rpm. The electrolyte was comprised of $Pb(NO_3)_2$ + 0.1 M HNO_3 + 0.04 M NaF and the Pb^{2+} concentration varied at 0.02, 0.1, 0.3, 0.5 and 1 M. The PbO_2 coatings were galvanostatically electroplated at the current densities of 5, 10, 20, 40, 60, 100 and 200 mA/cm^2 (Amount of charge for each deposition = 200 mA/cm^2 · min). It should be pointed out that due to the limitation of Pb^{2+} concentration, only two current densities: 5 mA/cm^2 (for 40 min) and 10 mA/cm^2 (for 20 min) were employed at 0.02 M Pb^{2+} to prepare PbO_2 coatings.

The electrolyte selection is to obtain β-PbO_2 and its composition is similar to that reported in Ref. [21,23,24] The addition of NaF is to promote nucleation of lead dioxide and control the growth of lead dioxide crystal.[13,25] Moreover, it has been reported that the use of F^- stabilizes the lead dioxide coating, improves adhesion and also inhibits oxygen evolution.[2,26] In all deposition experiments, the applied potential (in the range of 1.91 V to 3.37 V) increased with increasing current density and with decreasing Pb^{2+} concentration. To avoid the reduction of PbO_2 surface by chemical reaction with water, after each deposition, the PbO_2 sample was taken out immediately from the bath and rinsed with ethanol for 3 seconds, then washed ultrasonically for 5 min in a beaker containing 50 mL ethanol, followed by drying with cool air. It is noted that no oxygen bubble was observed during the electrodeposition of PbO_2 coating, except for PbO_2 deposited at 100 and 200 mA/cm^2 from electrolyte containing 0.1 M Pb^{2+} that resulted in a porous, flower-like microstructure. For Pb^{2+} concentrations from 0.3 M to 1 M, in all cases no oxygen bubble was observed. The current efficiency estimated from Faraday's law was about 100% in these cases.

Physicochemical characterization.— An environmental scanning electron microscope (Quanta 200F, FEI) was used to observe the surface morphology of the as-prepared Ti substrates and PbO_2 coatings. X-ray diffraction data were collected using a Bruker D2 X-ray diffractometer with Cu K_α radiation (λ = 1.54056 Å).

Results and Discussion

Ti/SnO_2-Sb substrate.— The surface morphology of an as-polished Ti coupon is shown in Fig. 1a. After being etched in the boiling oxalic acid, the physical appearance of Ti coupon was matte-silver in color and the surface was rough (Fig. 1b). Such a rough surface morphology favors the electrodeposition of the interlayer SnO_2-Sb [21] and improves the adherence of the coating. As can be seen in Fig. 1c, the as-prepared Ti/SnO_2-Sb substrate reveals many "mud-cracks", a typical morphology observed by other researchers.[27,28] The SnO_2-Sb layers were compact and intimate with the underlying Ti substrate. Fig. 1d is a cross-sectional SEM image of the Ti/SnO_2-Sb substrate with the interlayer being 1–2 μm thick. It should be noted that the cracks in the SnO_2-Sb layer (Fig. 1d) were caused during the mechanical grinding and polishing procedure. The SnO_2-Sb interlayer on Ti can significantly promote the subsequent electrochemical deposition of PbO_2 coatings. Moreover, the application of SnO_2-Sb interlayer is reported to have increased electrode's chemical stability, enhanced electrocatalytic activity and greatly prolonged service life of the electrodes.[9,22]

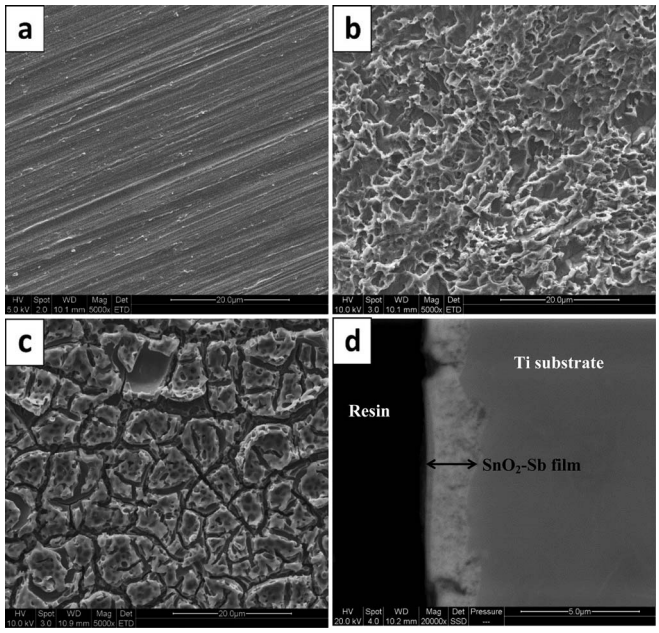

Figure 1. SEM images for (a) the as-polished Ti coupon; (b) as-etched Ti coupon; (c) SnO_2-Sb film deposited on the Ti/SnO_2-Sb substrate and (d) the cross-section of SnO_2-Sb film (thickness of 1–2 μm).

XRD analysis of the PbO_2 coatings.— The influence of current density on the phase composition of PbO_2 coatings deposited on the Ti/SnO_2-Sb substrates was determined by X-ray diffraction (XRD). Fig. 2 shows the XRD patterns of the PbO_2 coatings obtained from the electrolyte of 0.5 M $Pb(NO_3)_2$ + 0.1 M HNO_3 + 0.04 M NaF at varied current densities of 5, 10, 20, 40, 60, 100 and 200 mA/cm^2 (amount of charge for each deposition = 200 mA/cm^2 · min). The diffractograms clearly show some characteristic reflections of β-PbO_2 with a tetrag-

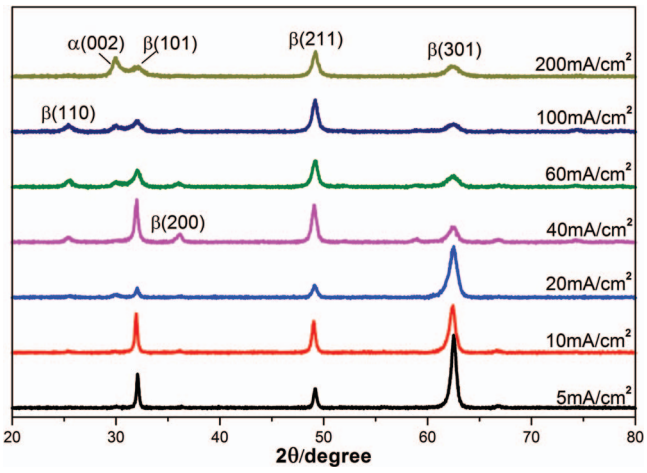

Figure 2. XRD diffractograms of the PbO_2 coatings deposited at various current densities. Electrolyte: 0.5 M $Pb(NO_3)_2$ + 0.1 M HNO_3 + 0.04 M NaF. Amount of charge for each deposition = 200 mA/cm^2 · min.

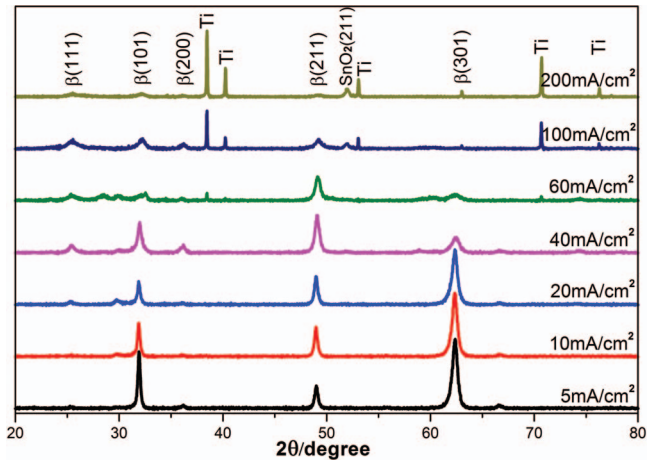

Figure 3. XRD diffractograms of the PbO_2 coatings deposited at various current densities. Electrolyte: 0.1 M $Pb(NO_3)_2$ + 0.1 M HNO_3 + 0.04 M NaF. Amount of charge for each deposition = 200 mA/cm^2 · min.

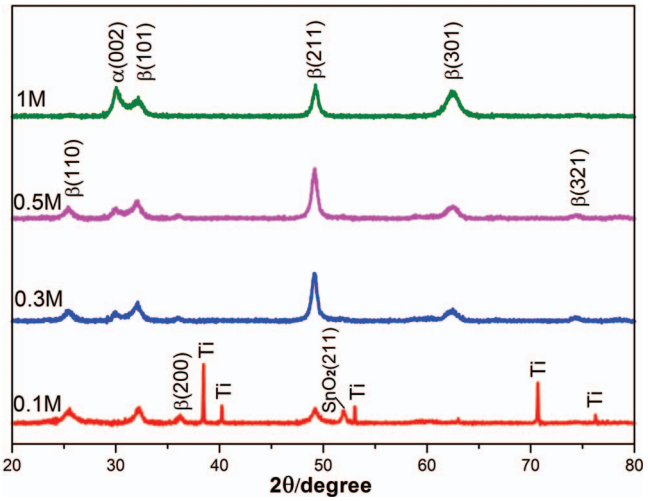

Figure 4. XRD diffractograms of the PbO_2 coatings deposited in electrolyte of $Pb(NO_3)_2$ + 0.1 M HNO_3 + 0.04 M NaF at various Pb^{2+} concentrations. Current density: 100 mA/cm^2, deposition time: 2 min.

onal structure, in accordance with the literature data.[2] Three strong diffraction peaks of β (101), β (211) and β (301) at 32.1°, 49.2° and 62.4° were identified, respectively. The XRD patterns of PbO_2 coatings at low current densities (i.e. 5, 10 and 20 mA/cm^2) are similar and exhibit a β (301) texture. At a higher current density of 40 mA/cm^2, two strong peaks of β (101) and β (211) planes are observed. Further increasing the current density results in an apparent texture - the (211) peak dominates. The existence of such a preferential orientation for crystallite growth has also been reported in the literature,[29,30] although the specific preferential crystallographic planes may vary in different cases. It should be noted that a weak yet distinguishable peak at 30.0° was detected in the coatings obtained at 60, 100 and 200 mA/cm^2, and can be indexed to (002) plane of α-PbO_2. In most cases, the PbO_2 films deposited in this study were a mixture of α- and β- phases except for the low current densities (≤ 40 mA/cm^2). This phenomenon is in good agreement with the other reports in the literature.[15]

The solution concentration interplays with current density for PbO_2 deposition. In this study we investigated the effect of current density on the deposition of PbO_2 when the solution concentration is low. Fig. 3 shows the diffractograms of the PbO_2 coatings deposited from the electrolyte of 0.1 M $Pb(NO_3)_2$ + 0.1 M HNO_3 + 0.04 M NaF at various current densities. In the case of low current densities (5, 10 and 20 mA/cm^2), all the samples present a significant preferential orientation of β (301) and this is identical to that obtained at a Pb^{2+} concentration ≤ 1 M (see Fig. 1 for 0.5 M Pb^{2+} concentration). In other words, the Pb^{2+} concentration seems to have limited effect on the crystallite texture if the deposition current density is low. In contrast, when the deposition current density increased up to 40 and 60 mA/cm^2, the PbO_2 coatings exhibited a β (211) texture. Further increasing the current density resulted in a pronounced change of the XRD patterns. The sharp peaks of 38.5°, 70.8° and 51.8° detected in the 100 and 200 mA/cm^2 coatings were indexed to the α-Ti phase and the (211) plane of the SnO_2 interlayer, respectively. The physical appearance of these deposits was porous, matte-brown in color, and can be easily removed by ultrasonic washing due to poor adhesion. The PbO_2 deposited at an even lower Pb^{2+} concentration of 0.02 M under current density of 10 mA/cm^2 (for 20 min) presented an identical physical appearance.

We speculated that 0.1 M Pb^{2+} concentration is too low for effective deposition of PbO_2 at an intermediate-to-high current density. We also intended to investigate whether it is possible to deposit PbO_2 coatings under a high current density and the minimum Pb^{2+} concentration in the electrolyte required for the effective deposition. Fig. 4 presents the XRD diffractograms of PbO_2 coatings deposited at a current density of 100 mA/cm^2 for 2 min from the electrolyte of $Pb(NO_3)_2$ + 0.1 M HNO_3 + 0.04 M NaF with various Pb^{2+} concentrations from 0.1 M to 1 M. Strong peaks of Ti/SnO_2-Sb substrate were detected when the Pb^{2+} concentration in the electrolyte is 0.1 M. This is because at a high current density, the mass transfer of Pb^{2+} ions becomes the limiting step. At a low Pb^{2+} concentration of 0.1 M, concentration polarization becomes extremely severe at the electrode surface, and ad-atoms can no longer reach the equilibrium position during PbO_2 deposition. Meanwhile, most of the applied current density is spent for O_2 evolution, instead of the deposition of PbO_2. Thus the PbO_2 film obtained is porous and loosely attached to the substrate, which fails to fully cover the substrate. At a higher Pb^{2+} concentration, the mass transfer of Pb^{2+} is faster and the concentration polarization at the electrode surface is limited, which results in relatively uniform and dense PbO_2 deposition. As can be seen in Fig. 4, the XRD patterns of PbO_2 film deposited at a higher Pb^{2+} concentration of 0.3, 0.5 and 1 M all presented a preferred orientation of β (211). In addition, at 1 M Pb^{2+} concentration, the peak indexed to the plane of α (002) becomes pronounced. The emergence of α-PbO_2 phase is in good agreement with the literature.[31] As reported by Velichenko et al.,[31] in an acid electrolyte, where β-PbO2 is the main deposit, the amount of α-phase impurity increases with increasing potential in the kinetically controlled region.

As observed in our experiments, the PbO_2 coatings demonstrated different crystallographic orientations depending on either current density or Pb^{2+} concentration. When deposited at a current density < 40 mA/cm^2, the phase composition of the coating is independent of Pb^{2+} concentration and presents a preferential crystal orientation of β (301). At a higher current density > 40 mA/cm^2, the obtained PbO_2 coatings have a preferential crystal orientation of β (211) texture. At an even higher current density (e.g. 200 mA/cm^2), the α-PbO_2 (002) emerges. This phenomenon has also been reported in the literature, that is, the formation of α-PbO_2 is favored by a relatively high current density while β-PbO_2 is favored at low current densities.[15,32] At a high current density of 100 or 200 mA/cm^2, the limitation of Pb^{2+} concentration may cause severe concentration polarization at the surface of electrode, and result in extremely porous PbO_2 deposits, which fail to fully cover the substrates.

Table I summarizes the crystallite size data of the PbO_2 coatings obtained at varied current density of 5, 10, 20, 40, 60, 100 and 200 mA/cm^2 from the electrolyte: $Pb(NO_3)_2$ + 0.1 M HNO_3 + 0.04 M NaF at different Pb^{2+} concentrations of 0.02, 0.1, 0.3, 0.5 and 1 M. The crystallite size is estimated from the width of β (211) diffraction peak at half maximum intensity (FWHM) using the Scherrer formula.[33] When increasing the current density from 20 to 40 mA/cm^2, a substantial decrease of the PbO_2 crystal size is observed. The crystallite size decreased from 25 ± 2 nm at a current density of 5∼20 mA/cm^2

Table I. PbO_2 Crystallite sizes at various current density. Electrolyte: $Pb(NO_3)_2$ + 0.1 M HNO_3 + 0.04 M NaF. Pb^{2+} concentration varied from 0.02 to 1M. Amount of charge for each deposition = 200 mA/cm^2 · min.

Conditions	5 mA/cm^2	10 mA/cm^2	20 mA/cm^2	40 mA/cm^2	60 mA/cm^2	100 mA/cm^2	200 mA/cm^2
0.02 M	26	Porous	-	-	-	-	-
0.1 M	23	25	24	17	15	Porous	Porous
0.3 M	26	25	27	16	15	14	15
0.5 M	24	22	23	16	14	15	14
1 M	25	24	24	18	14	14	14

to 16 ± 1 nm at 40 mA/cm^2. Further increasing the current density to 60∼200 mA/cm^2 only slightly decreased the crystallite size to 14∼15 nm. The current density-dependent growth of PbO_2 crystallites has also been reported by others.[13,15,16] In general, a low current density (i.e. low electrodeposition potential) favors the growth of PbO_2 crystallites and this is in good agreement with Ref. [31]. By contrast, high current density favors nucleation of crystallites, and the relatively smaller crystal sizes resulted from a massive nucleation that leads to increasing polycrystallinity and smaller crystallites as the presence of more neighbor nuclei limiting the extent of growth.[29] As indicated in Table I, the Pb^{2+} concentration seems to have limited effect on the growth of PbO_2 crystallites.

SEM characterization of PbO_2 deposits.— Fig. 5 shows SEM micrographs of the PbO_2 coatings deposited from 0.5 M $Pb(NO_3)_2$ + 0.1 M HNO_3 + 0.04 M NaF bath at varied current densities yet with identical charge amount (200 mA/cm^2 · min). It is revealed that PbO_2 deposited at low current densities gave rise to larger deposits with clear edges. At 5 mA/cm^2, the PbO_2 coating presented an irregular pebble-shaped surface with deposits being 3–5 μm in size (Fig. 5a). Increasing the current density to 10 and 20 mA/cm^2 did not change the morphology (images identical to Fig. 5a). At a higher current density of 40 mA/cm^2, the PbO_2 deposits were smaller and spheroidal (Fig. 5b). Further increasing the current density significantly changed the coating morphology. As shown in Fig. 5c, the PbO_2 obtained at 60 mA/cm^2 illustrated a rough surface morphology with smaller barley-like deposits (Fig. 5f: high-magnification). The PbO_2 coating prepared at 100 mA/cm^2 (Fig. 5d) had highly dense spindle shaped deposits. When the current density increased to 200 mA/cm^2 (Fig. 5e), the coating appeared to be rather dense, and were of spheroid shape 10 μm in diameter. The high-magnification image reveals that the spheroidal deposit is indeed an aggregate of many nano-sized grains (inset, Fig. 5e).

The deposit morphology is significantly different if the Pb^{2+} concentration in the electrolyte is low. Fig. 6 shows the SEM micrographs

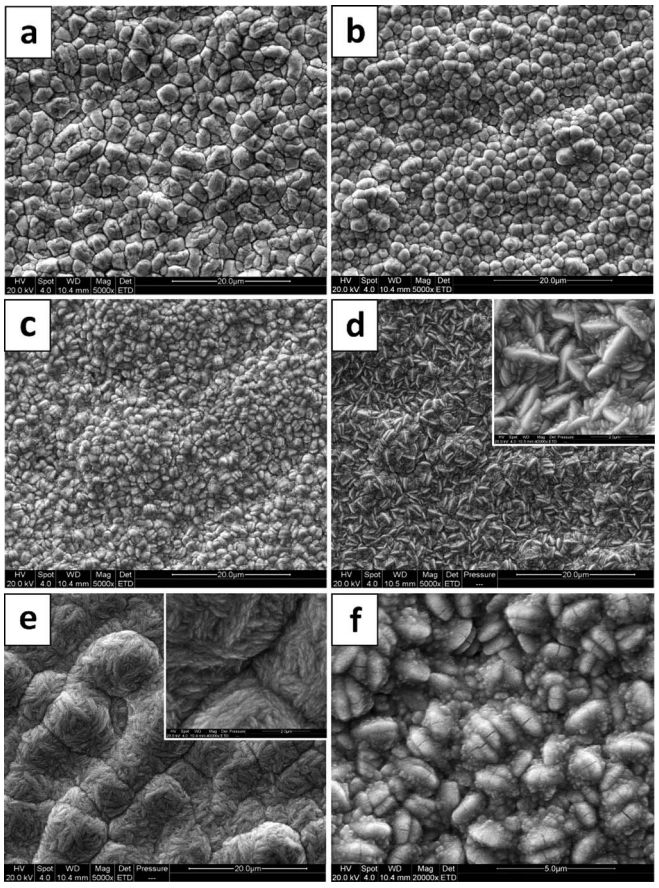

Figure 5. SEM images of the PbO_2 coatings deposited at: (a) 5 mA/cm^2 for 40 min, (b) 40 mA/cm^2 for 5 min, (c) 60 mA/cm^2 for 3 min 20 s, (d) 100 mA/cm^2 for 2 min, (e) 200 mA/cm^2 for 1 min and (f) high-magnification of (c). Electrolyte: 0.5 M $Pb(NO_3)_2$ + 0.1 M HNO_3 + 0.04 M NaF. Insets are high-magnification images.

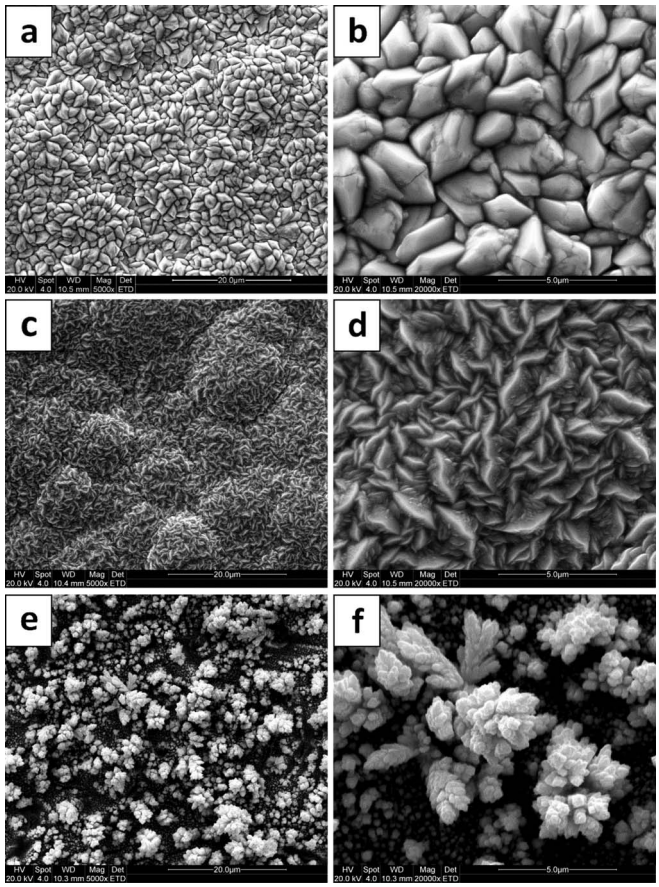

Figure 6. SEM images of the PbO_2 coatings deposited at : (a) and (b) 40 mA/cm^2 for 5 min, (c) and (d) 60 mA/cm^2 for 3 min 20 s, (e) and (f) 100 mA/cm^2 for 2 min. Electrolyte: 0.1 M $Pb(NO_3)_2$ + 0.1 M HNO_3 + 0.04 M NaF.

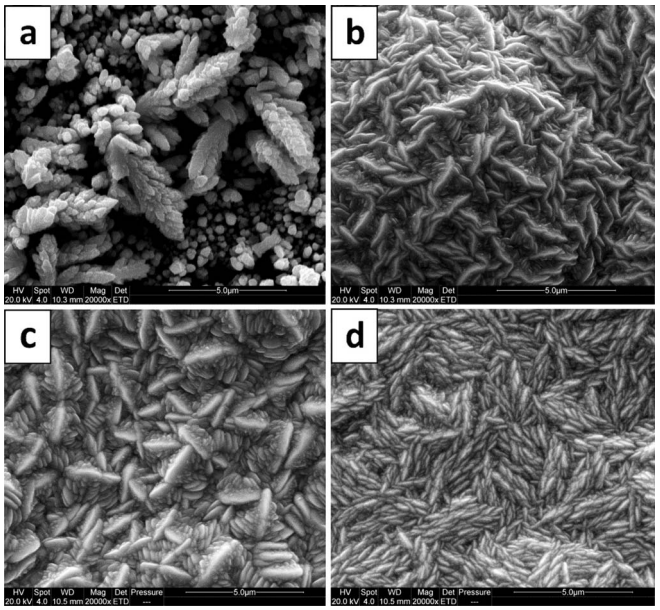

Figure 7. SEM images of the PbO_2 coatings deposited in electrolyte of $Pb(NO_3)_2$ + 0.1 M HNO_3 + 0.04 M NaF at various Pb^{2+} concentrations: (a) 0.1 M, (b) 0.3 M, (c) 0.5 M and (d) 1 M. Current density: 100 mA/cm^2, deposition time: 2 min.

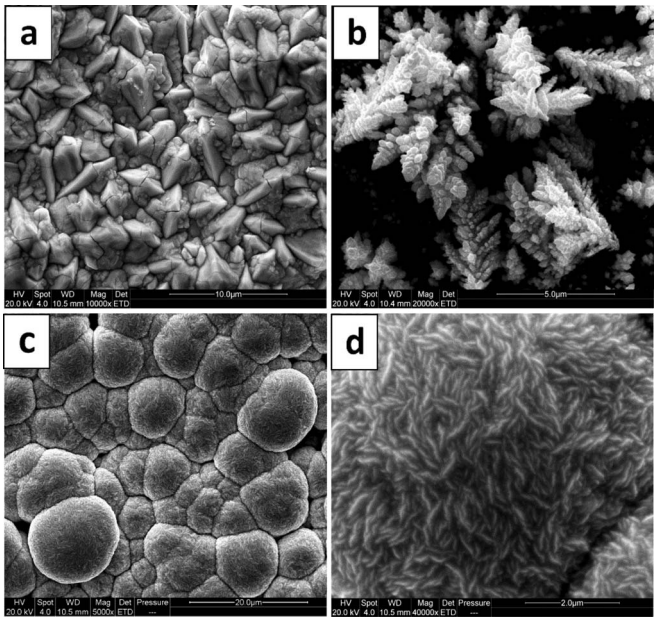

Figure 8. SEM images of the PbO_2 coatings deposited in electrolyte of $Pb(NO_3)_2$ + 0.1 M HNO_3 + 0.04 M NaF at various Pb^{2+} concentrations and current densities: (a) 0.02 M Pb^{2+}, 5 mA/cm^2 for 40 min; (b) 0.02 M Pb^{2+}, 10 mA/cm^2 for 20 min; (c) and (d) 0.3 M Pb^{2+}, 200 mA/cm^2 for 1 min.

of the PbO_2 coatings deposited from 0.1 M $Pb(NO_3)_2$ + 0.1 M HNO_3 + 0.04 M NaF bath at various current densities. It is noted that the PbO_2 deposited at < 40 mA/cm^2 were pebble-shaped and distributed uniformly with clear edges (identical to Fig. 5a). Increasing current density to 40 mA/cm^2 resulted in smaller and angular-shaped deposits (Figs. 6a and 6b). As shown in Figs. 6c and 6d, the 60 mA/cm^2 deposited PbO_2 film presented a rough surface morphology composed of worm-shaped particles aligned in various directions. An increase of the current density to 100 mA/cm^2 caused a pronounced change in the morphology and the deposited PbO_2 (Figs. 6e and 6f) revealed a porous, flower-like structure growing along the vertical direction. A similar outward growth of PbO_2 deposits at high current densities has been reported by Shen et al.[13] It is noted that the 200 mA/cm^2 deposited PbO_2 coating demonstrated the same porous, flower-like structure. It should be pointed out that oxygen bubbles were observed during the electrodeposition of these two porous PbO_2 coatings when deposited at 100 and 200 mA/cm^2 from electrolyte containing 0.1 M Pb^{2+}.

The effect of Pb^{2+} concentration in the electroplating bath on the PbO_2 morphology was presented in Fig. 7. It is clear that Pb^{2+} concentration has a significant influence on the morphology of the deposited PbO_2 coatings. At a low Pb^{2+} concentration of 0.1 M, the PbO_2 film (Fig. 7a) had a porous, flower-like structure growing outward (Figs. 7a, 6e and 6f were taken from the same sample). This porous PbO_2 coating was matte-brown and can be easily removed by ultrasonic washing. This explains why the peaks from Ti and SnO_2 were detected in the corresponding XRD patterns (Figs. 3 and 4). At a higher Pb^{2+} concentration of 0.3 M, the PbO_2 film deposited (Fig. 7b) appeared to be worm-shaped, which is similar to the structure observed in Fig. 6c and 6d (except the coating here were denser). By further increasing the Pb^{2+} concentration, spindle-shape deposits were observed at 0.5 M (Fig. 7c), while highly dense deposits made of nano-sized grains were revealed at 1 M Pb^{2+} concentration (Fig. 7d).

The PbO_2 coatings obtained from the very low Pb^{2+} concentration electrolyte are shown in Fig. 8. In the case of 0.02 M Pb^{2+}, we only investigated two current densities: 5 and 10 mA/cm^2. In comparison with the PbO_2 coatings obtained at higher Pb^{2+} concentrations, the 5 mA/cm^2-deposited PbO_2 at 0.02 M Pb^{2+} was angular in shape and much smaller in size, as illustrated in Fig. 8a. Porous, flower-like structure was observed at 10 mA/cm^2 deposited PbO_2 under the Pb^{2+} concentration of 0.02 M (Fig. 8b). It should be pointed out that no oxygen bubbles were observed during the electrodeposition of this porous coating (10 mA/cm^2, 0.02 M). It is speculated that the porous, flower-like microstructure can be obtained by either employing very low Pb^{2+} concentration at extremely low current density or applying extremely high current density but at high concentration. The SEM images of PbO_2 film deposited in the electrolyte of 0.3 M $Pb(NO_3)_2$ + 0.1 M HNO_3 + 0.04 M NaF at current density of 200 mA/cm^2 for 1 min were shown in Figs. 8c and 8d. A polygonal-shaped morphology with some spheroidal deposits growing outward was observed in Fig. 8c. Such deposits consist of many nano-sized particles of worm-shaped structure (Fig. 8d). It is noted that this worm-shaped structure has also been observed in Fig. 6d (0.1 M, 60 mA/cm^2) and Fig. 7b (0.3 M, 100 mA/cm^2), except the size of the structure decreased significantly with increasing current density. It is also found that the XRD patterns of these three worm-shaped PbO_2 coatings were identical and repeatable.

It is evident that the physicochemical characteristics of PbO_2 coatings largely depend on the current density and Pb^{2+} concentration in bath, which determine the deposition mechanism. At a current density < 40 mA/cm^2, charge transfer process is the limiting step and the process is current controlled. If the Pb^{2+}concentration in the electroplating bath is not extremely low, the Pb^{2+} ions arriving at the electrode surface would be sufficient. In this case, the PbO_2 deposits present well-formed, pebble-shaped morphology with larger crystallite sizes. Under these conditions, all the charges are spent for the formation of PbO_2 deposits and the current efficiency could reach 100%. At a higher current density (e.g. 100 mA/cm^2), mass transfer becomes rate controlling. In other words, the process is diffusion controlled. Concentration polarization occurs at the electrode surface. Nucleation becomes dominant, resulting in a smaller grain size. Under such electroplating conditions, Pb^{2+} ions may fail to find the equilibrium position during PbO_2 deposition process, and as a result non-uniform morphology is observed (Fig. 7a). With a further increase in the current density, the concentration polarization of Pb^{2+} becomes extremely severe, and a secondary reaction (i.e. oxygen evolution) occurs. Most of the applied charges are consumed in oxygen evolution, which largely decreases the current efficiency. The PbO_2 coatings

obtained under these conditions show porous, flower-like morphology, and the deposition is favorable for outward growth.

It has been proposed that the electrodeposition process has two distinct steps.[15] The first step is the formation of nuclei of the new phase and their growth into crystals (crystallization). Once the substrate is fully covered by a few layers of this oxide, the second step occurs by the thickening of the layer into macroscopic deposits. Before PbO_2 phase nucleates and then grows, necessary chemical reaction steps must be completed to form colloidal PbO_2 phase. The sequence of chemical steps toward the formation of crystalline PbO_2 has long been the subject of much interest and speculation. A plausible reaction mechanism is that proposed by Velichenkoi et al. who suggest that the electrodeposition process involves absorbed OH as a key reaction intermediate:[34,35]

$$H_2O \rightarrow OH_{ads} + H^+ + e^- \quad [1]$$

$$Pb^{2+} + OH_{ads} \rightarrow Pb(OH)^{2+} \quad [2]$$

$$Pb(OH)^{2+} + H_2O \rightarrow PbO_2 + 3H^+ + e^- \quad [3]$$

Eq. 3 may be further divided into the following two steps:

$$Pb(OH)^{2+} + H_2O \rightarrow Pb(OH)_2{}^{2+} + H^+ + e^- \quad [3a]$$

$$Pb(OH)_2{}^{2+} \rightarrow PbO_2 + 2H^+ \quad [3b]$$

In this mechanism, Pb^{2+} ions first react with the previously chemisorbed OH_{ads} on the electrode surface to form a soluble intermediate species $Pb(OH)^{2+}$, followed by being further oxidized into PbO_2 via Eq. 3. Alternatively the soluble intermediate containing Pb(III) is oxidized into $Pb(OH)_2{}^{2+}$ via Eq. 3a, and this Pb(IV)-containing intermediate is decomposed, via Eq. 3b, to form colloidal PbO_2 particles that crystallize on the electrode. At low potentials the second charge transfer stage (Eq. 3a) is rate determining, while at higher potential region the Pb^{2+} diffusion becomes rate controlling in the PbO_2 formation process. It is logical to assume that the colloidal PbO_2 particles arrive at the electrode in a rather random manner until the entire coating coverage is achieved. Afterwards, the crystallization event of new PbO_2 nuclei may occur on certain previously-formed PbO_2 crystalites with favorable orientation. It is also likely that the growth along certain orientations is more favorable than others. This may explain why the coatings demonstrate a β (301) orientation and a pebble-shaped morphology when the current density is < 40 mA/cm^2.

The incorporation of ionic additives such as F^- in the electrodeposition bath does not alter the deposition mechanism; it only changes the electrodeposition kinetics.[35] It may be hypothesized that the physical adsorption of ionic species (negatively charged) on the growing oxide accelerates the transport of the colloidal oxide particles toward the anode. It was reported that the doping of fluoride promotes the formation of pure β-PbO_2, as compared to un-doped PbO_2 coating.[35] However, the other factors such as current density and Pb^{2+} concentration in the electroplating bath may well offset this effect. For example, a higher Pb^{2+} concentration and/or a higher current density lead to the emergence of α-PbO_2 phase (Figs. 2 and 4).

Conclusions

PbO_2 coatings were electrodeposited on Ti/SnO_2-Sb substrates using constant current density in an acidic nitrate solution. It is evident that Pb^{2+} concentration and current density affect the PbO_2 coatings in a synergic manner. In most cases, a mixture of α + β-PbO_2 phase was obtained except at a low current density. At a current density < 40 mA/cm^2, the coating exhibited a pure β-PbO_2 phase and the concentration seems to have insignificant effect on the morphology and crystallographic orientation of the PbO_2 coatings. In all these PbO_2 coatings, the β phase exhibited a (301) texture and the coatings had a pebble-shaped morphology. On the other hand, at a higher current density, the PbO_2 deposit exhibited a dominant β-PbO_2 phase with a minor α-PbO_2 phase present. In these cases, the morphology of the deposits is sensitive to the corresponding current density and Pb^{2+} concentration. The PbO_2 coatings exhibited a porous flower-like morphology under the deposition at 100 mA/cm^2 in 0.1 M Pb^{2+} bath, while the deposit morphology changed to worm-like and spindle-like if the Pb^{2+} concentration increased to 0.3 M and 0.5 M respectively. This study indicates that either a sufficiently high concentration or low current density is necessary in order to obtain a compact and dense PbO_2 deposit. Otherwise non-uniform or porous deposits would result from severe concentration polarization at the electrode surface.

Acknowledgments

Hailian Bi acknowledges the support from China Scholarship Council (CSC) for providing a doctoral scholarship for her study at the University of Auckland.

References

1. D. Pletcherb and F. C. Walsh, *Industrial Electrochemistry*, Chapman and Hall, London, UK (1990).
2. X. Li, D. Pletcher, and F. C. Walsh, *Chem Soc Rev*, **40**, 3879 (2011).
3. E. R. Kötz and S. Stucki, *Journal of Electroanalytical Chemistry and Interfacial Electrochemistry*, **228**, 407 (1987).
4. A. A. Babak, R. Amadelli, A. De Battisti, and V. N. Fateev, *Electrochim Acta*, **39**, 1597 (1994).
5. M. Clancy, C. J. Bettles, A. Stuart, and N. Birbilis, *Hydrometallurgy*, **131–132**, 144 (2013).
6. A. N. Nikoloski and M. J. Barmi, *Hydrometallurgy*, **137**, 45 (2013).
7. K. C. Narasimham and H. V. K. Udupa, *J Electrochem Soc*, **123**, 1294 (1976).
8. D. Pletcher and S. J. D. Tait, *J Appl Electrochem*, **11**, 493 (1981).
9. S. Song, L. Zhan, Z. He, L. Lin, J. Tu, Z. Zhang, J. Chen, and L. Xu, *J Hazard Mater*, **175**, 614 (2010).
10. J. Iniesta, E. Expósito, J. González-García, V. Montiel, and A. Aldaz, *J Electrochem Soc*, **149**, D57 (2002).
11. J. Iniesta, J. González-GarcıÍa, E. Expósito, V. Montiel, and A. Aldaz, *Water Res*, **35**, 3291 (2001).
12. S. R. Ellis, N. A. Hampson, M. C. Ball, and F. Wilkinson, *J Appl Electrochem*, **16**, 159 (1986).
13. P. K. Shen and X. L. Wei, *Electrochim Acta*, **48**, 1743 (2003).
14. X. Li, D. Pletcher, and F. C. Walsh, *Electrochim Acta*, **54**, 4688 (2009).
15. N. Yu, L. Gao, S. Zhao, and Z. Wang, *Electrochim Acta*, **54**, 3835 (2009).
16. S. Ghasemi, M. F. Mousavi, and M. Shamsipur, *Electrochim Acta*, **53**, 459 (2007).
17. K. T. Kawagoe and D. C. Johnson, *J Electrochem Soc*, **141**, 3404 (1994).
18. X. Yang, R. Zou, F. Huo, D. Cai, and D. Xiao, *J Hazard Mater*, **164**, 367 (2009).
19. Y. Zheng, W. Su, S. Chen, X. Wu, and X. Chen, *Chem Eng J*, **174**, 304 (2011).
20. M. Zhou, Q. Dai, L. Lei, C. Ma, and D. Wang, *Environ Sci Technol*, **39**, 363 (2005).
21. H. Bi, C. Yu, W. Gao, and P. Cao, *Electrochim Acta*, **113**, 446 (2013).
22. Y. Wang, B. Gu, W. Xu, and L. Lu, *Rare Metal Mat Eng*, **36**, 874 (2007).
23. H. An, H. Cui, W. Zhang, J. Zhai, Y. Qian, X. Xie, and Q. Li, *Chem Eng J*, **209**, 86 (2012).
24. J. Cao, H. Zhao, F. Cao, J. Zhang, and C. Cao, *Electrochim Acta*, **54**, 2595 (2009).
25. A. B. Velichenko, D. V. Girenko, S. V. Kovalyov, A. N. Gnatenko, R. Amadelli, and F. I. Danilov, *J Electroanal Chem*, **454**, 203 (1998).
26. J. Cao, H. Zhao, F. Cao, and J. Zhang, *Electrochim Acta*, **52**, 7870 (2007).
27. A. R. Zeradjanin, F. La Mantia, J. Masa, and W. Schuhmann, *Electrochim Acta*, **82**, 408 (2012).
28. B. Adams, M. Tian, and A. Chen, *Electrochim Acta*, **54**, 1491 (2009).
29. I. Sirés, C. T. J. Low, C. Ponce-de-León, and F. C. Walsh, *Electrochim Acta*, **55**, 2163 (2010).
30. D. Devilliers, M. T. Dinh Thi, E. Mahé, V. Dauriac, and N. Lequeux, *J Electroanal Chem*, **573**, 227 (2004).
31. A. B. Velichenko, R. Amadelli, A. Benedetti, D. V. Girenko, S. V. Kovalyov, and F. I. Danilov, *J Electrochem Soc*, **149**, C445 (2002).
32. J. P. Carr, N. A. Hampson, and R. Taylor, *Journal of Electroanalytical Chemistry and Interfacial Electrochemistry*, **27**, 109 (1970).
33. A. L. Patterson, *Phys Rev*, **56**, 978 (1939).
34. A. B. Velichenko, E. A. Baranova, D. V. Girenko, R. Amadelli, S. V. Kovalev, and F. I. Danilov, *Russ J Electrochem*, **39**, 615 (2003).
35. A. B. Velichenko and D. Devilliers, *J Fluorine Chem*, **128**, 269 (2007).